Development of a hybrid element to model intralaminar damage in thick composite plates under impact loading

Ldjoudi Manseri, Pablo Navarro, Olivier Dorival, Steven Marguet, Bassam Mahmoud, Jean-François Ferrero

Version of Record: https://www.sciencedirect.com/science/article/pii/S1359836821004108
Manuscript_70cae60d06314d7c9ee5fab2a0df18e5

Development of a hybrid element to model intralaminar damage in thick composite plates under impact loading

L. Manseri[a], P. Navarro[a], O. Dorival[a,b], S. Marguet[a], B. Mahmoud[c], J.-F. Ferrero[a]

[a] *Université de Toulouse, Institut Clément Ader, UMR CNRS 5312, INSA/ISAE/Mines Albi/UPS, 3 rue Caroline Aigle, 31400 Toulouse, FRANCE*
[b] *Icam, site de Toulouse, 75 avenue de Grande Bretagne, 31300 Toulouse, FRANCE*
[c] *University of Balamand, Deir El-Balamand, El-Koura, LEBANON*

Abstract

This article deals with the development of a new intralaminar interface in order to extend the *semi-continuous strategy* already developed by the authors for impacts on thin composite laminates to thicker ones. Based on medium experimental observations scale, the new interface introduced aims at capturing transverse resin cracks occurring between fibre bundles of a unidirectional ply. The new element is implemented in the commercial finite element software Radioss®. Results of impact simulations performed on thick HTA7-913 plates (various thicknesses) are compared with experimental ones, and show good agreements in terms of both damage sizes and load-displacement curves.

Keywords: unidirectional composites, thick laminate, impact loading, intralaminar rupture, interface model, damage mechanics, semi-continuous strategy

1. Introduction

Composite materials are increasingly used, especially in the aeronautical industry due to their high resistance to weight ratio. However, during their life cycle, they can undergo several impacts at different velocities, that can create barely visible damages [1] [2]. This damage (BVID) is caused by several situations such as a low velocity impact during the maintenance of an aircraft. The impact generates a small indentation at the surface which is often non visible at naked-eye but with extended matrix cracking and delamination inside the laminate. This phenomenon has been studied by many researchers and many methods to detect it as [3] where Bragg sensors are used or [4] in which non-destructive method are described to reconstruct the damage.

The first definition of a low-velocity impact was given by [5] who is also one of the precursors of the first precise damage cartographies. With those pictures, the three damage mechanisms for the resin of composite materials are identified : intralaminar damage (between the fibres), delamination (between two plies) and transverse failure (across the thickness of the sample).

Several authors studied the influence of many impact parameters on the response of the composite structure such as the impact energy [6] or the impact time (*i.e.* the contact duration between the impactor and the structure) [7]. Geometrical parameters such as the impact area to composite thickness ratio was found to have a strong influence on the rupture mode [8]. Composite thickness is known to be a key parameter as it directly influences proportion of bending and shear stresses in the structure. This thickness effect is even more pronounced for glass/epoxy composites as explained in

[9], and was studied by many other researchers such as Abrate [10], who claimed that initiation of matrix cracking is related to structure thickness. In fact, the higher the thickness, the closer these cracks get to the impact zone. Conversely, for thin laminates, matrix cracks begin at the opposite of the impacted zone and then propagate through the thickness towards the impacted face. The damage cone is reversed in this case.

Delamination is known to be the most penalizing damage [11] as it generally leads to a stiffness loss of the structure that then becomes unusable. In many studies, delamination is initiated by transverse cracks that develop inside the ply between bundles of fibres [12]. The cracks then propagate through the thickness until they reach the interfaces between the plies, what leads to the initiation of inter-ply delamination. The coupling between transverse cracking and delamination is very difficult to catch, despite some attempts such as [13]. Moreover, the effect of the thickness brings complexity, because the mechanisms between an impact on a thin plate and a thicker one are not the same as described in [14]. Many studies showed that the structures which have a high angle difference between two successive plies are more sensitive to delaminate. In the same idea, [15] showed that draping consecutively many plies in the same direction reduces the impact performance of the laminate.

In order to develop predictive models, the key question is about the modelling scale required to both correctly capture the physics of damage, and allow reasonable calculation time. [16] and [17] made a meaningful

review of the strategies used to represent the interfaces in a composite plate. Among the various techniques developed, cohesive zone models have shown great potential. Fine scale enables to represent the decohesion between the fibres and the resin [18] but leads to unreasonably expensive computation time. Macro-scale models that allows "fast" calculations for large structures (in most cases by using 2D element because in this case the thickness is very small compared to the other dimensions) generally suffer difficulties for fine damage representation. Then, dimensioning composite structure for impacts is done with macroscopic criteria such as in [19], [20] or [21]. In between, meso-scale models are developed with the idea that the entire laminate can be represented by a combination of plies and interfaces [22]. In theses approaches, many plies in the same direction can be modelled by only one numerical ply and the interface between plies is represented by 2D or 3D cohesive element. Other researchers used specific meshes in which intralaminar damageable interfaces are specifically put in the regions where cracks are likely to occur [23].

In order to represent the damage mechanism starting from the intra-laminar initiation to the inter-laminar propagation, many modellings have been conducted. They catch the initiation and the propagation of the cracks at the interface between two adjacent plies with a good accuracy by using specific damage initiation and propagation laws [24, 25]. The *Discrete Ply Modelling Method* developed by Bouvet [23] is based on a discrete damage such as the one developed in [26]. This allows to model with a very fine accuracy both the behaviour of the intralaminar and interlaminar interfaces

in thin or thick composite plates under an impact load. One of the key point of the model is in the coupling between intralaminar and interlaminar elements. Despite the accuracy of the results, the mesh required is often complex and the method is time consuming due to small interface sizes that lead to important drop in the time step.

Unlike inter-laminar interfaces that are now commonly used, intra-laminar elements are not widespread. Three major modelling approaches use them : the bi-phasic approach [27], the intra-laminar load reversal damage [28], and the statistical approach [29]. Their advantage is in the precision of the results but the equations that drive them are complex and the simulations are computationally heavy to perform.

In the same lines as [23], Navarro et al. [30] developed the *semi-continuous model* based on the dissociation of the fibres and resin mechanical behaviours. The bundle of fibres are represented by rod elements and the resin is modelled by specific shell elements that allows to stabilize the fibres. This approach was used to represent composite plates submitted to impact loads. Initially developed for woven laminates, it was mainly fuelled by Pascal et al. [31] that allowed to model the interface between two woven layers. Further, Mahmoud et al. [32] also used this strategy and adapted it to unidirectional (UD) laminate structures. The model was developed for thin plates and provided a good correlation between the experimental tests and the simulations. However damage mechanisms that occur in thick laminates can not be captured without accounting for the specificity of the physics in such structures.

The aim of this paper is to extend the *semi-continuous model* to thick composite laminates. Therefore, based on the work previously exposed, a new interface is developed and disposed between rod elements to represent the matrix transverse cracking. In this article, will be presented the finite element formulation, the coupling between intralaminar and interlaminar damages and the effect of the out-of-plane compression on the delamination. Those developments are implemented in commercial finite elements software Radioss®. The interface is validated by comparisons with both quasi-static and impact tests carried out on plates with various thicknesses and impact velocities. The results are compared to the experimental ones and show good predictive performances.

2. Development of an intralaminar interface for the *semi-continuous model*

In this section, based on experimental observations, the principle of the interface is exposed and element is implemented in the *semi-continuous model*.

2.1. Experimental observations

Thick unidirectional laminate structures have typical damage surfaces specifically solicited during development of damage mechanisms. Indeed, during an impact loading at high velocity (high energy), damage starts with matrix cracks and followed by propagation of delamination, eventually leading to fibre breakage. The latter quickly leads to the ruin of the structure. But at low velocities, only the resin breaks as seen in Figure

1 in which the test was performed with a drop weight with an impactor of 2 kg at 3 m/s. This preliminary test was performed with the same conditions and set up than will be described in Section 3.This figure shows the tomography of an impacted structure composed of HTA7-913 composite laminate $[0_4/90_4]_2/0_2]_s$ after 9J impact test. This tomography was done by the authors at the *Institut Clément Ader* with a micro-tomograph with a voxel resolution of 0.06 mm^3.

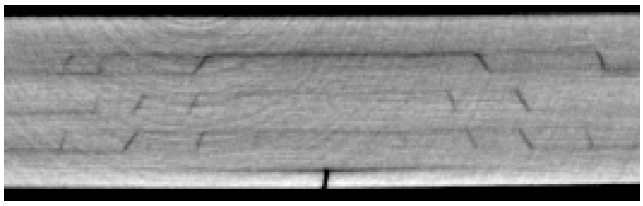

Figure 1: Matrix cracks and delamination in a composite laminate under impact loading at 3 m/s

Matrix cracks and inter-ply delamination are clearly identifiable in Figure 1. The one which is on the bottom of the laminate is at 90°. This means that it appears because of the plate's bending. The other cracks are approximately at 45° which represents a damage that occurred by shear. Based on the mechanisms observed, the semi-continuous model is completed in the following with the development of a specific interface element. The aim is to capture transverse cracking and the coupling with the propagation of inter-ply delamination. In the semi-continuous model, delamination has already been addressed by an interlaminar damageable interface element detailed in [31]. The objective of this paper is to introduce another interface that will capture intralaminar matrix cracks, and to calibrate the coupling

between transverse matrix cracking and interply delamination.

2.2. Development of the element

The new element is a user-defined element implemented in Radioss®. The behaviour of the element is written inside a user Fortran subroutine that is called at each time step of the explicit calculation. The inputs are the translational and rotational velocities of the nodes. The outputs of this routine are the loads and momentums on each node. The behaviour of this element is described in this section.

2.2.1. Geometry

The previous section showed that during an impact in thick laminates, multiple matrix cracks occur between bundles of fibres. They are of discrete nature (no diffuse cracking here) and are often referred to as *transverse cracks*. In order to model as a discrete phenomenon, a new intralaminar interface is included in the *semi-continuous model* as described in Figure 2. This interface is placed between the UD elements composed of {rods+shell+interlaminar interface}.

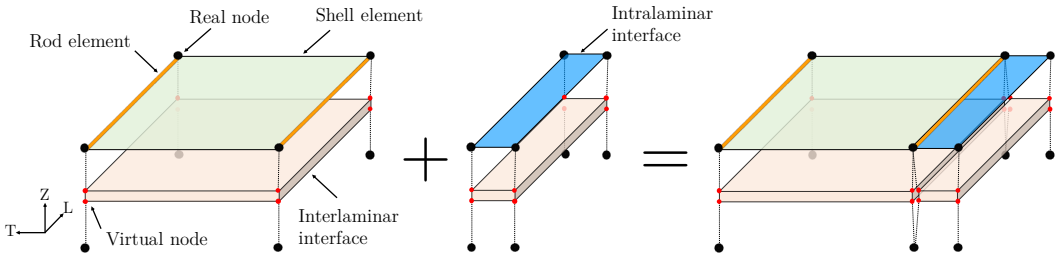

Figure 2: Modelling of the intralaminar interface interspersed between the UD elements

The size of this interface element is 1 mm long and 10 μm wide. The length is constrained by the length of neighbours UD {rods+shell+interlaminar interface} element. The width has to be small enough for shear stresses to quickly lead to the rupture but large enough to avoid an important decrease of the time step.

2.2.2. Finite element formulation

The element geometry requires 4 nodes. Radioss® user elements are 8-nodes BRICK elements, only 4 of them were used for the intralaminar interface as shown in Figure 3.

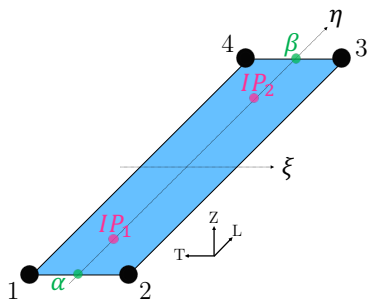

Figure 3: Location of the integration points in the intralaminar element

Since the width is 100 times larger than the length, only two integration points are needed for the calculation and they are placed in the largest direction of the element (*i.e.* in the fibre direction). IP_1 is at $\left(0, \frac{-1}{\sqrt{3}}\right)$ and IP_2 at $\left(0, \frac{1}{\sqrt{3}}\right)$ in the element local coordinate system $(\boldsymbol{\xi}, \boldsymbol{\eta})$.

Let (α, β) denote the middle points of short element edges. Displacement $\mathbf{u}$ along η is interpolated from displacements of $\mathbf{u}_\alpha$ and $\mathbf{u}_\beta$ with shape

functions that are expressed only in the η-direction. Shape functions do not depend on ξ due to very small variation along this direction. The displacement of any node in the element is then given by :

$$\mathbf{u}(\xi,\eta) = \mathbf{u}(\eta) = \frac{1-\eta}{2}\mathbf{u}_\alpha + \frac{1+\eta}{2}\mathbf{u}_\beta \tag{1}$$

The interface element is driven by displacement jumps and rotational jumps of the nodes. Their expression is then based on the node velocities jumps $\dot{\delta}_k$ that between left and right nodes of the element. They are expressed in the ply coordinate system $(\mathbf{L},\mathbf{T},\mathbf{Z})$ (see Figure 3) as follows:

$$\dot{\boldsymbol{\delta}}_\mathbf{k} = \dot{\mathbf{u}}_\mathbf{R} - \dot{\mathbf{u}}_\mathbf{L} = \begin{pmatrix} \dot{\delta}_{k,l} \\ \dot{\delta}_{k,t} \\ \dot{\delta}_{k,z} \end{pmatrix} \text{ with } \begin{cases} \text{if } k=\alpha \quad \text{then } (R,L)=(2,1) \\ \text{if } k=\beta \quad \text{then } (R,L)=(3,4) \end{cases} \tag{2}$$

Velocity jumps are interpolated at integration points as:

$$\dot{\boldsymbol{\delta}}_\mathbf{i} = \frac{1-\eta_i}{2}\dot{\boldsymbol{\delta}}_\alpha + \frac{1+\eta_i}{2}\dot{\boldsymbol{\delta}}_\beta \text{ with } i = \{IP_1, IP_2\} \tag{3}$$

Finally, displacement jumps for the next time step are simply computed by integrating Eq. (3):

$$\boldsymbol{\delta}_\mathbf{i}\big|_{t+\Delta t} = \boldsymbol{\delta}_\mathbf{i}\big|_t + \Delta t.\dot{\boldsymbol{\delta}}_\mathbf{i} \tag{4}$$

The same approach is done for rotational jumps $\dot{\boldsymbol{\delta}}\boldsymbol{\theta}_\mathbf{i}$ with $k=(\alpha,\beta)$. Stresses are then computed at integration point. The stress matrix $[\sigma^\delta]$ induced by displacement jumps can be written as:

$$\left[\sigma^{\delta}\right] = \begin{pmatrix} \sigma^{\delta}_{tt} \\ \sigma^{\delta}_{lt} \\ \sigma^{\delta}_{zt} \end{pmatrix} = \begin{pmatrix} K_{tt}.\delta_t \\ K_{lt}.\delta_l \\ K_{zt}.\delta_z \end{pmatrix} \tag{5}$$

In a similar way, rotational jumps generate bending stresses $[\sigma^{\theta}]$ that are given by:

$$\left[\sigma^{\theta}\right] = \begin{pmatrix} \sigma^{\theta}_{tt} \\ \sigma^{\theta}_{lt} \\ \sigma^{\theta}_{zt} \end{pmatrix} = \begin{pmatrix} K^{r}_{tt}.\delta\theta_t \\ K^{r}_{lt}.\delta\theta_l \\ 0 \end{pmatrix} \tag{6}$$

The interface stiffness parameters $(K_{tt}, K_{lt}, K_{zt}, K^r_{tt}, K^r_{lt})$ will be identified in the next section.

In order to capture transverse cracking due to complex stress state, classical damageable cohesive law can be used to degrade stiffness (Figure 4).

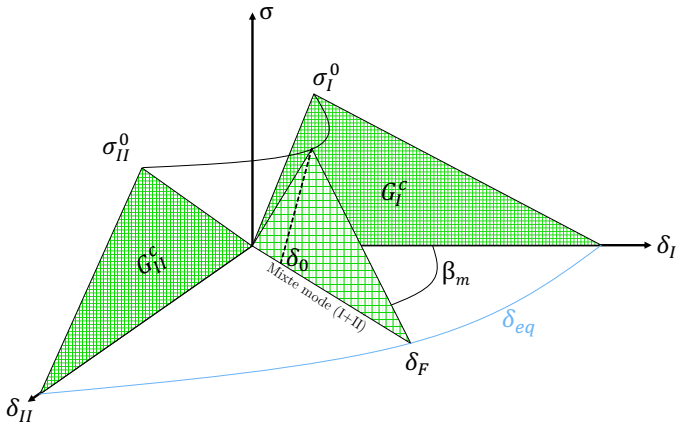

Figure 4: Bilinear cohesive law for the intralaminar interface damage

The first step is the linear elastic behaviour until the stress initiation (σ^0_I and σ^0_{II}). The initiation is based on a quadratic criterion:

$$\left(\frac{\sigma_{tt}}{\sigma_I^0}\right)^2 + \left(\frac{\sigma_{zt}}{\sigma_{II}^0}\right)^2 = 1 \tag{7}$$

Consequently, the second part of the bilinear law represents the progressive damage of the element with a rupture characterized by a drop of the stress. Damage evolution is driven by a single damage variable d progressively growing from 0 (no damage of the element) to 1 (element totally damaged). To compute it, it is necessary to get the equivalent displacement jumps for opening mode (mode I) and shear mode (mode II); they are expressed by the following expressions:

$$\begin{cases} \delta_I = \delta_t + \left|\frac{e}{2}\delta\theta_l\right| & \text{for Mode I} \\ \delta_{II} = |\delta_z| & \text{for Mode II} \end{cases} \tag{8}$$

with e the ply thickness.

Damage evolution is classically based on energy release rates according to:

$$\left(\frac{G_I}{G_{Ic}}\right)^\alpha + \left(\frac{G_{II}}{G_{IIc}}\right)^\alpha = 1 \text{ , with } \alpha = 1 \tag{9}$$

Thanks to this relation, damage variable d can be computed by:

$$d = \frac{\delta_F}{\delta}\left(\frac{\delta - \delta_0}{\delta_F - \delta_0}\right)_{\delta_0 \leq \delta \leq \delta_F} \tag{10}$$

with $\delta = \sqrt{\delta_I^2 + \delta_{II}^2}$ the actual equivalent displacement jump, δ_0 the equivalent displacement jump at initiation and δ_F the equivalent displacement jump at rupture. Stresses due to the displacement jumps are then given by:

$$\left[\sigma^{\delta^*}\right] = (1-d)\left[\sigma^{\delta}\right] \tag{11}$$

For the sake of simplicity, it was chosen to use the same damage variable to degrade rotational stiffnesses.

2.2.3. Coupling between intralaminar and interlaminar damages

In order to initiate more accurately the appearance of delamination, coupling between interlaminar damage (delamination) and damage of the new intralaminar element is a key step. However Radioss® does not allow for a given element to "discuss" with the neighbours. A trick is to use the θ_z degree of freedom (out-of-plane rotation), that is used neither in the UD element formulation nor in the interface element formulation. When the intralaminar interface is broken, a pulse signal is sent through θ_z degree of freedom to each node j of the element in the form of a momentum M_z^j according to :

$$M_z^j = -2I_j \frac{\Delta\dot{\theta}_z^0}{\Delta t} \text{ with } j = \{1,2,3,4\} \tag{12}$$

with I_j the "inertia" of the node j, $\Delta\dot{\theta}_z^0$ the value of the rotational velocity gap needed to induce the pulse and Δt the time step.

This pulse is sent from the intralaminar element through a momentum and as a results it is detected by the interlaminar interface through the angular velocities of the UD element nodes. Nevertheless, each node of the intralaminar interface is linked to 4 neighbours elements (either UD elements or intralaminar elements) and one needs to know exactly where to start the initiation of delamination. Experimentally, delamination starts simultane-

ously in both sides of the transverse crack. For this reason the choice is made to initiate delamination in the two UD elements located to the left and the right of the intralaminar interface. In the UD element coordinate system (see Figure 5), the following criterion is used for the initiation of delamination:

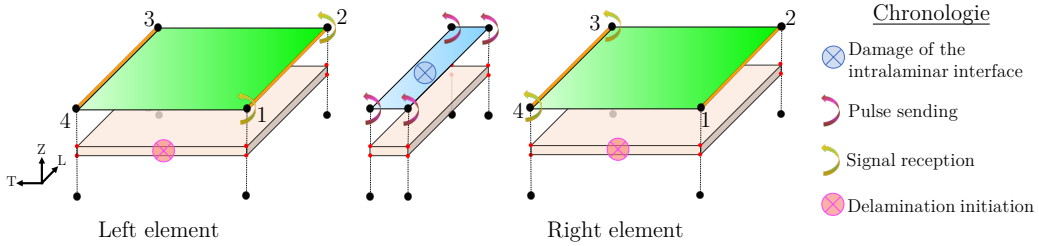

Figure 5: Connexion between intralaminar and interlaminar interfaces

$$\text{If} \begin{cases} \left\|\dot{\theta}_z|_t^1 - \dot{\theta}_z|_{t-\Delta t}^1\right\| \geq \Delta\dot{\theta}_z^0 \;\&\; \left\|\dot{\theta}_z|_t^2 - \dot{\theta}_z|_{t-\Delta t}^2\right\| \geq \Delta\dot{\theta}_z^0 \\ \text{Or} \\ \left\|\dot{\theta}_z|_t^3 - \dot{\theta}_z|_{t-\Delta t}^3\right\| \geq \Delta\dot{\theta}_z^0 \;\&\; \left\|\dot{\theta}_z|_t^4 - \dot{\theta}_z|_{t-\Delta t}^4\right\| \geq \Delta\dot{\theta}_z^0 \end{cases} \text{then } \delta_0 = \delta\big|_t \tag{13}$$

In words, this equation states that when intralaminar element breaks, then delamination initiates in the left and the right interlaminar interfaces.

2.2.4. Inclusion of the out-of-plane compression

Unlike thin laminates, the stress state in thick laminates involves at the same time bending tensile stress (σ_l, σ_t), shear stress (σ_{lt}) and compressive stress in the thickness direction (σ_z). During the impact, the central zone under the impactor is undergoing compressive stress due to the important

thickness of the laminate. This prevents the delamination from occurring by shearing until a given threshold. For this reason, the stress initiation in Mode II for the interlaminar interface τ_{II} is computed as a function of out-of-plane stress. The following expression, known as *Mohr-Coulomb criterion*, describes the evolution of this threshold:

$$\tau_{II} = \sigma_{II}^0 + \left|\eta.\sigma_z\right|, \text{ with } \eta = -\frac{1}{\tan\left(2\phi\right)} \tag{14}$$

with σ_{II}^0 the classical stress initiation in mode II, ϕ the angle of intralaminar cracks with respect to the horizontal axis and σ_z the out-of-plane interlaminar stress in the local coordinate system (as shown in Figure 5). The energy release rate is also recalculated by taking into account the previous modification. For mode II, the new energy release rate $\mathcal{G}_{IIc}$ is given by:

$$\mathcal{G}_{IIc} = G_{IIc}\left[1 - 2\eta\frac{\sigma_z}{\sigma_{II}^{max}} + \left(\eta\frac{\sigma_z}{\sigma_{II}^{max}}\right)^2\right] \tag{15}$$

As a consequence, the inclusion of the intralaminar interface has an influence on the global behaviour of the model, especially on the interlaminar interface, whose parameters need to be re-identified.

Finally, the new version of the model can be seen as a hybrid element. Indeed, this intralaminar element is represented by a shell and all computations are done at the integration points. However, its behaviour is identical to a cohesive element and accounts for out-of-plane stress. This new approach adds 11 new parameters : 5 stiffnesses ($K_{tt}, K_{lt}, K_{zt}, K_{tt}^r, K_{lt}^r$), 2 initiation stresses for mode I (σ_I^0) and mode II (σ_{II}^0), 2 energy release rates for mode I

(G_{Ic}) and mode II (G_{IIc}), 1 value for the angular velocity gap for the pulse ($\Delta\dot{\theta}_z^0$) and 1 value for the angle for the intralaminar cracks direction (ϕ). All of them need to be determined. As already mentioned, the parameters of the interlaminar interface must also be re-identified as a consequence of the coupling between interlaminar and intralaminar phenomena.

2.3. Identification of the parameters

2.3.1. Stiffness parameters

First of all, the stiffness parameters are derived from a physical meaning. K_{tt} is the tensile stiffness that represents the interface mode I, K_{lt} and K_{zt} are the shear stiffnesses of the element (*i.e.* in mode II), K_{tt}^r and K_{lt}^r are two parameters needed to compute the bending stresses from node rotations:

$$\begin{cases} K_{tt} = \dfrac{E_m}{e} \\ K_{lt} = K_{zt} = \dfrac{G_m}{e} \\ K_{tt}^r = K_{lt}^r = K_{tt}.\dfrac{e_p}{2} \end{cases} \tag{16}$$

with E_m the resin elastic modulus, G_m the resin shear modulus, $e = 10\ \mu m$ the width of the intralaminar element and e_p the thickness of the composite ply.

2.3.2. Crack angle identification

The angle of the intralaminar interface was studied by some authors such as Aubry [33]. The angle reveals the type of the main solicitation that leads to the crack. Indeed, an angle close to 90° shows a rupture caused by bending. However, an angle close to 45° means that the crack appeared by

out-of-plan shear. The mean angle found in the literature is $\phi = 57°$.

Figure 6 displays crack angles for HTA7-913 laminate whose the stacking sequence is $[0_4/90_4]_2/0_2]_s$, that was submitted to a 3 m/s impact loading. In this study, the average angle is a mean of all the angles inside the plies except the lower ply, because this parameter characterizes the angle of the matrix cracks induced by an out-of-plane loading, contrary to the lower one that undergoes a bending load.

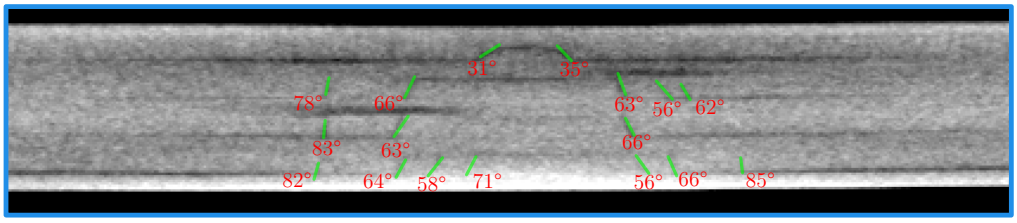

Figure 6: Micro-tomography of matrix cracks in $[0_4/90_4]_2/0_2]_s$ laminate under impact at 3 m/s

2.3.3. Identification of intralaminar interface parameters

After that, a tensile test is performed in order to obtain the stress initiation value in mode I for the intralaminar interface. The test is performed on a sample of HTA7-913 laminate. Its dimensions are 120x20 mm^2 and it is composed of 4 layers oriented at 90° (see Figure 7). The thickness of each layer is equal to 0.13 mm so the measured thickness of the sample is 0.52 mm. One side is clamped and the other side is subjected to an imposed displacement of 1.2 mm, at a speed of 0.1 mm/ms.

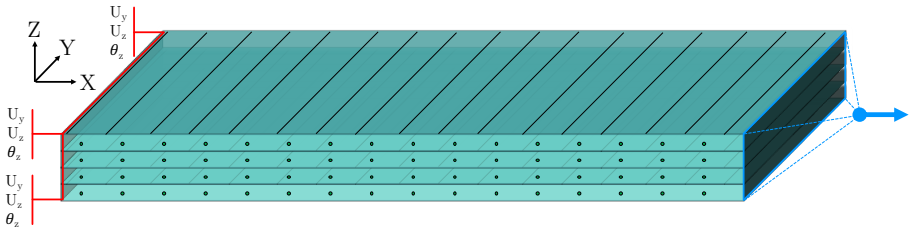

Figure 7: Tensile specimen constituted by four 90° layers

The tensile test is carried out until the final rupture of the sample. The value of σ_I^0, obtained by reverse identification (see Figure 8) in the numerical model is 72 MPa. The variation of the slope that is observed at the beginning is due to the initial positionning of the specimen inside of the clamping claws. Nevertheless, it has been checked with several other tests that it does not influence the validation of the parameters.

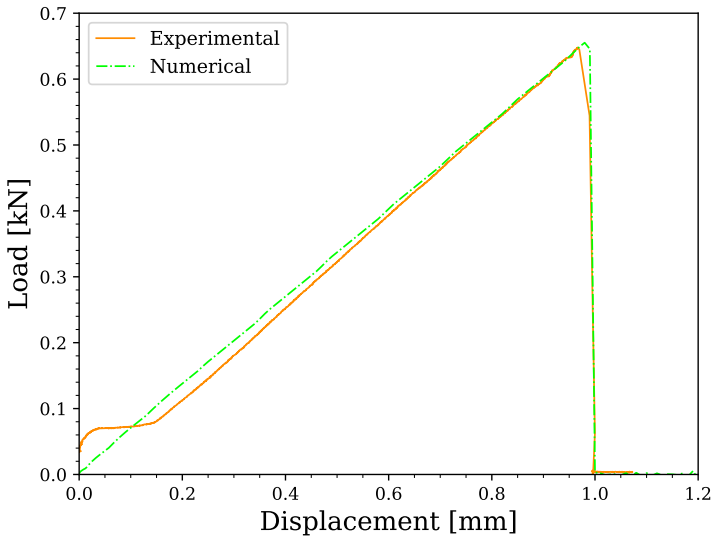

Figure 8: Comparison between experimental and numerical results for the tensile test at 90°

Once this parameter is fixed, the next step is to estimate the energy-release rate in mode I. Figure 8 shows that the specimen rupture is very brutal; damage initiation quickly leads to the complete rupture of the specimen. This means that G_{Ic} corresponds to the elastic energy stored until damage initiation. The value $G_{Ic} = 0.010 kJ/m^2$ is identified from the tensile tests previously presented.

In a similar way, the parameters for mode II are identified by using quasi-static indentation on HTA7-913 plates.

3. Modelling of a thick laminate under a drop-weight impact tests

3.1. Material tested and stacking sequences

The material used in the study is HTA7-913 (carbon fibres + epoxyde resin) and is provided by *Hexcel* as a prepreg roll. This section will focus on drop weight impact tests performed on plates of 125x100 mm^2 dimension. The thickness depends on the stacking sequence detailed in Table 1. The objective here is to show the effect of the thickness on the initiation of the intralaminar cracks and its propagation into delamination.

Number of plies	**Stacking sequence**	**Notation**	**Thickness**
20	$[0_4/90_4/0_2]_s$	5P 0-90	2.60 mm
36	$[[0_4/90_4]_2/0_2]_s$	9P 0-90	4.68 mm
36	$[0_4/+45_4/90_4/-45_4/0_2]_s$	9P QI	4.68 mm
52	$[[0_4/90_4]_3/0_2]_s$	13P 0-90	6.76 mm

Table 1: Configurations used for the study

Those stacking sequences are composed by 0° and 90° plies in order to favour delamination in the laminate in the case of "5P 0-90", "9P 0-90" and "13P 0-90" (see Figure 9).

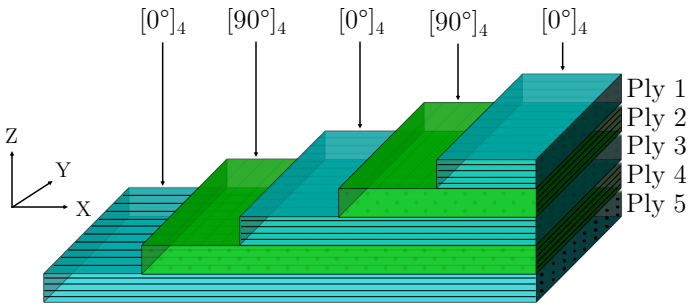

Figure 9: Stacking sequence used for 5P 0-90

However, it is also interesting to validate the model with more classical orientations. To this aim, a quasi-isotropic laminate (QI) is also studied. It is composed by 36 plies with a stacking sequences composed by ±45° plies : $[0_4/+45_4/90_4/-45_4/0_2]_s$ referred to as "9P-QI" (see Figure 10).

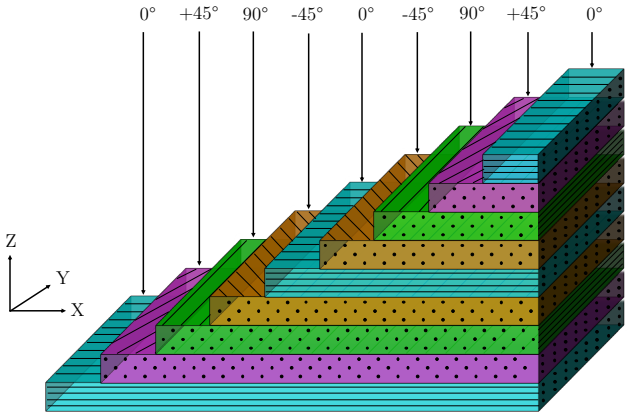

Figure 10: Stacking sequence used for 9P-QI

The plates are manufactured by draping consecutively prepreg sheets on top of each other. The final laminate is achieved by a cure cycle of 3 hours at 180 $°C$. Finally, the latter is cut to get the final plates with standard dimensions *i.e.* 125x100 mm^2. Those plates are impacted at different velocities: 3 m/s, 4 m/s and 5 m/s in order to understand the effect of the loading velocity on the damage mechanism. The tests are simulated with Radioss® by using the strategy developed above and then compared to the experimental ones. Concerning the numerical model, the plies are meshed by shell elements of 0.99x1.00 mm^2 and the intralaminar interfaces are meshed by the specific element developed in this paper with a dimension of 0.01x1.00 mm^2 as illustrated in Figure 11. The numerical plies are connected between them with kinematic bonding (option 'interface type 2' in Radioss®).

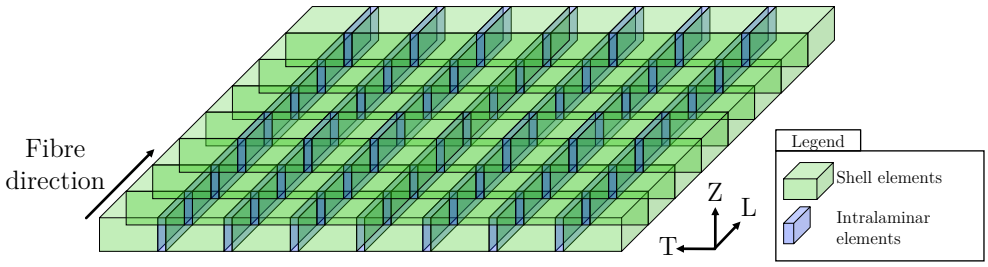

Figure 11: Mesh of the plies and interfaces in the model

The section below presents in a first part the case of "9P 0-90" at 3 m/s in details with the damage observed, the differences in absorbed energy with experimental tests, a model without intralaminar elements [32] and the new model. In the second part, others simulations are presented more succinctly.

3.2. Test set-up

The tests are performed with a drop weight machine. The impactor chosen has an hemispheric 16 mm diameter head and weights 2 kg. The composite sample is simply put onto a steel frame which size is 100x75 mm^2 as described in Figure 12. Each single ply has a thickness of 0.13 mm. The thicker the laminate, the more important the out-of-plane shear stress inside the resin between the bundle of fibres. Then, this allows to lead to brittle failures and also to figure out the interaction between the intralaminar and interlaminar cracks.

The acquisition of data is performed by a force sensor and a laser-based displacement sensor. The internal damages in the plate are analysed by X-ray tomography with a voxel size of 66 μm.

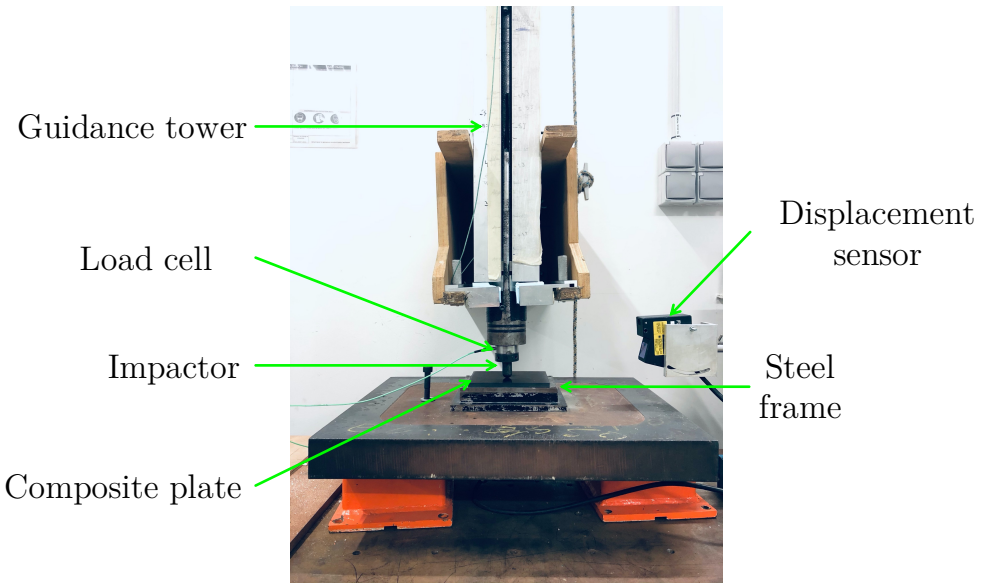

Figure 12: Experimental conditions of the impact tests

3.3. Results and discussion on "9P 0-90" at 3 m/s

This section presents the results of the tests and simulations that have been detailed in the previous sections. In order to validate the model and to justify the need of the intralaminar interface developed in this paper, the model is compared to the experimental results on one hand, and to a model without intralaminar elements on the other hand. Drop weight impacts are performed on all the stacking sequences that are previously presented and at 3 m/s, 4 m/s and 5 m/s. But for the sake of clarity, only one of them will be presented in details. Other results will be presented in the next section.

3.3.1. Load-displacement curves

The load-displacement curves for tests on "9P 0-90" at 3 m/s are shown in Figure 13.

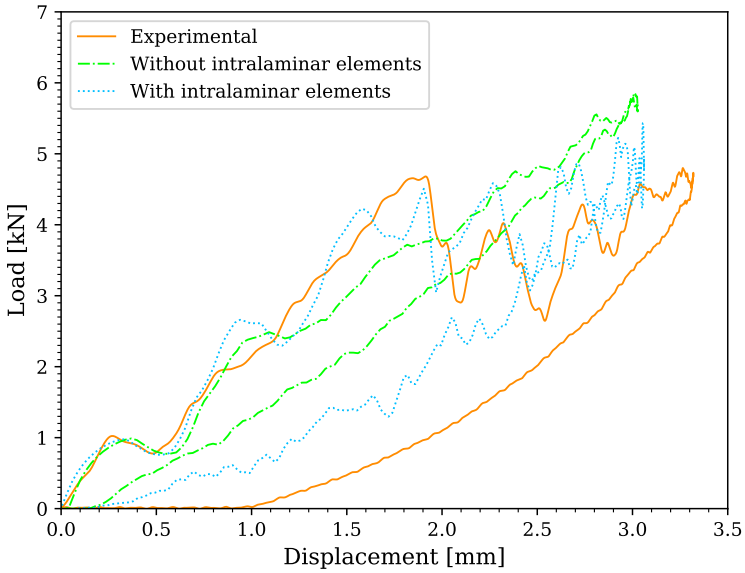

Figure 13: Load-displacement curves for the experimental test and the models with/out intralaminar elements (9P 0-90 at 3 m/s)

During the first step, both models follow the experimental curve and reproduce similar shock wave. However, the model without intralaminar interface increases until the impactor rebound and cannot capture the load drops occurring at 1.85 mm. As a consequence, the energy (area under the curve) is wrong. On the contrary, with the model with intralaminar interfaces, the behaviour is clearly better in terms of both energy and maximum displacement. The values are summarised in Table 2. Moreover, the sudden loss in the load at 1.8 mm is well represented and in right proportions compared to the experimental one.

—	*Experimental*	*Without intralaminar element*	*With intralaminar element*
Energy dissipated	5.82 J	1.69 J	3.85 J
Energy error	—	71%	34%
Maximum displacement	3.26 mm	2.79 mm	3.06 mm
Displacement error	—	15%	6%

Table 2: Comparison of dissipated energy and maximum displacement between the experimental results and two models with/out intralaminar interface element

3.3.2. Damage mechanisms

The load-time curves allow to identify the damage sequence as depicted in Figure 14. The figure shows that the sudden cracks occur at the right time in regards to the experimental curves. To the author knowledge, no clear experimental results concerning the chronology of the damage phenomena have been published in open literature; however, the simulation provides an interesting insight to understand the initiation and development of damage.

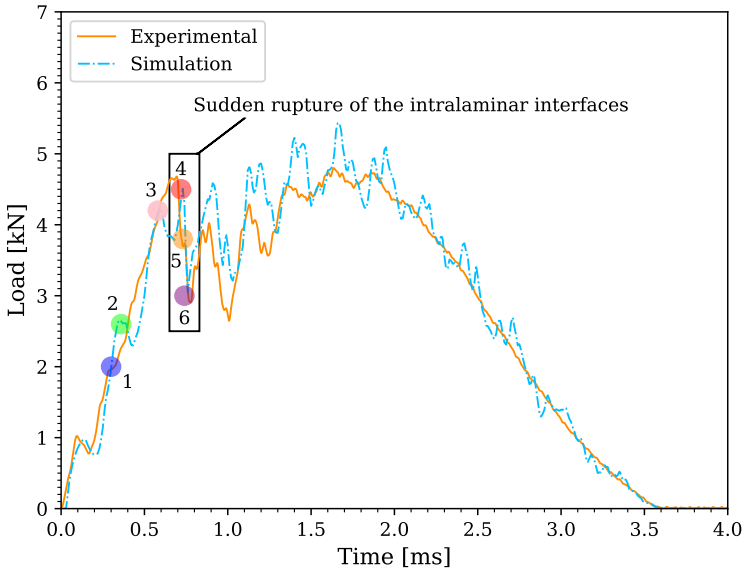

Figure 14: Load-time curves for the experimental test and the model with intralaminar elements

Figure 15 summarizes the numerical damage scenario. As we can see, there are different steps:

- **Step 1** : Intralaminar damage on the opposite side to the impact. Only one intralaminar elements row develops damage during the loading. This is caused by the bending of the lower ply that generates tensile stress on the lower ply, leading to a so-called tensile crack.

- **Step 2** : Some intralaminar elements break directly under the impactor, because of the local indentation of the resin caused by the impactor.

- **Step 3** : Delamination is initiated as a result of intralaminar broken elements.

- **Step 4** : Some intralaminar elements break in the 8^{th} ply and delamination go on propagating.

- **Step 5** : Some intralaminar elements of the 2^{nd} ply break, so the delamination is initiated through the laminate thickness. This is due to the high level of out-of-plane shear stresses in the resin (in the intralaminar elements in the model).

- **Step 6** : Damage in the upper plies and the lower ones converge at the center of the laminate.

The scenario identified above shows that the damage begins at the free surfaces of the laminate and join at the center for the stacking sequence considered here. For the sake of clarity, this very precise analysis was detailed only for the 9P 0-90 sample. However, the model is able to catch the damage scenario for thinner and thicker plates. Indeed, for thin specimens (such as for the case 5P 0-90) the damage still begins by a splitting at the opposite side of the impact then, due to the bending of the structure, the damage propagates in the thickness until it joins the ply that sees the impactor. Conversely, for thicker laminates like 13P 0-90, the damage begins also by the splitting of the opposite ply then the cracks appear alternatively in the half-superior side and the half-inferior side.

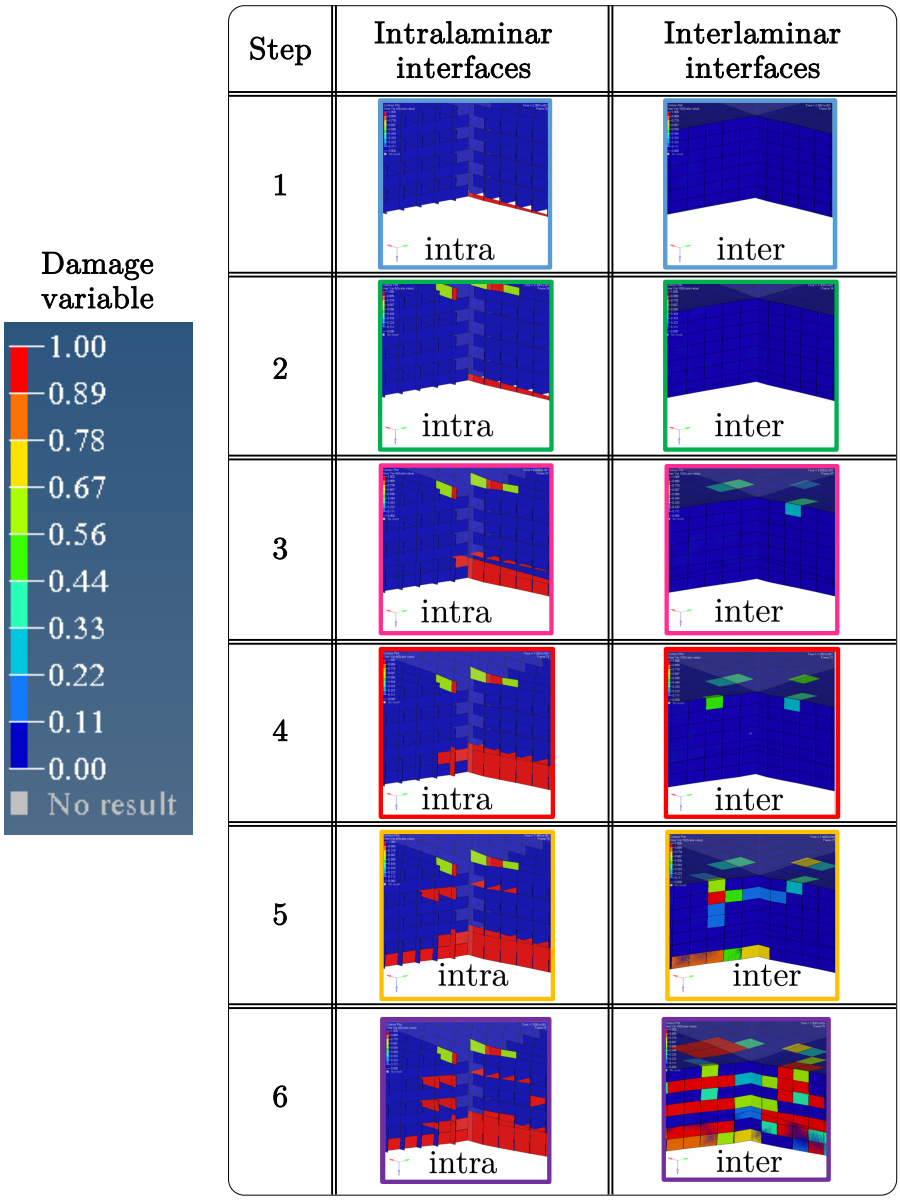

Figure 15: Numerical damage scenario of intralaminar and interlaminar interfaces

3.3.3. Intralaminar damage and delamination

Another way of validation is the use of X-ray tomography. Such analysis provides pictures of the *post-mortem* laminate sufficiently accurate to validate the damage resulting from the numerical model identified. Comparison between experimental and numerical results is shown in Figure 16. The plies numbering follows the same strategy as the one presented in Figure 9.

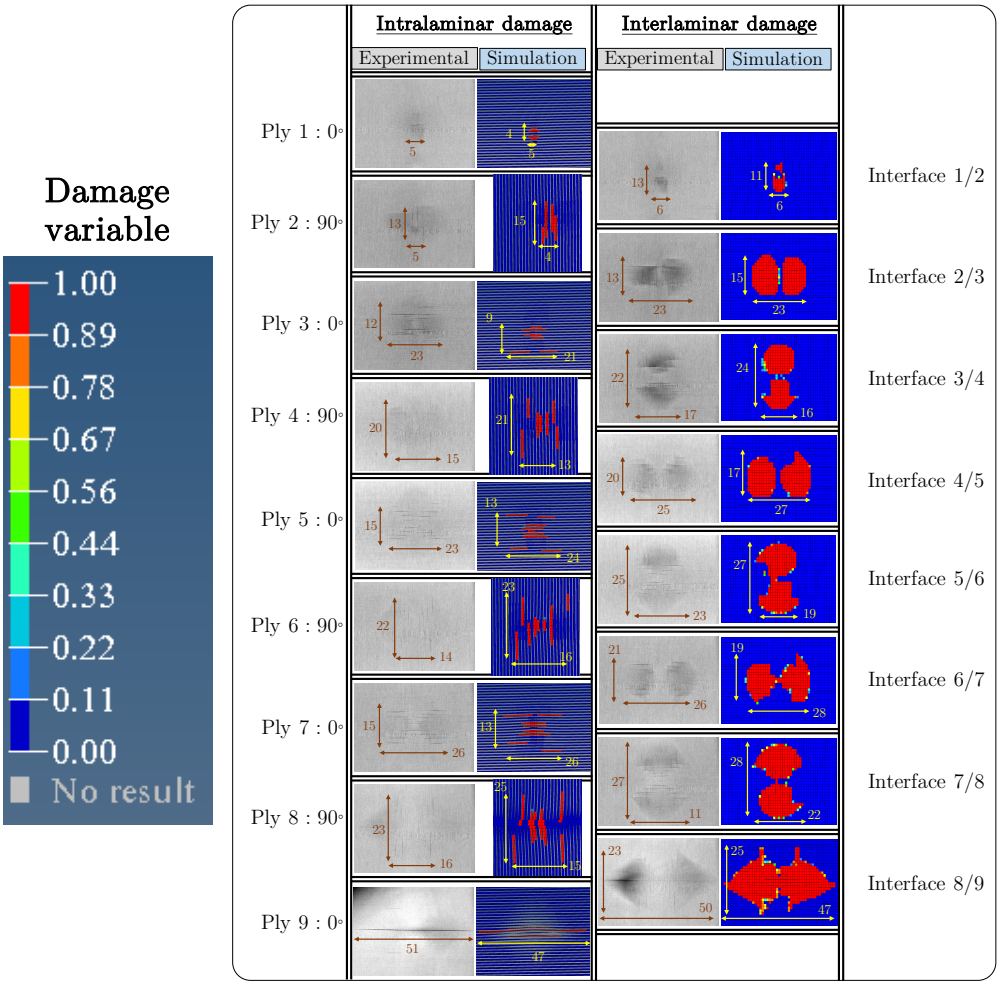

Figure 16: Comparison between experimental and numerical intralaminar damages and delaminations (in mm)

The damage experimentally observed is well captured by the model in terms of both shape and size. A typical "X-shape" of matrix cracks and "peanut shape" of delamination are represented with a good accuracy (less than 11% of error on delaminated areas). Furthermore, the analysis of the damage confirms what have been observed experimentally and described in the literature : delamination is initiated by intralaminar cracks, that manage the damage scenario. Thus the intralaminar element presented in this article has a key role in the representation of the degradation. The global *post-mortem* damage, that is depicted in Figure 17, also confirms the predictive aspect of the model. This shows the projected delaminated surfaces, extracted from Figure 16. Its aim is to have an idea of the overall scope of delamination.

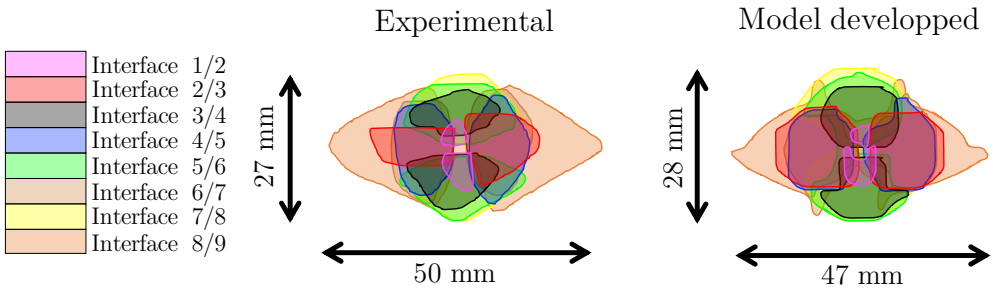

Figure 17: Comparison between experimental and numerical damage

3.4. Experimental and numerical comparison for other impact cases

This section will present the results of the simulations for the impacts on "5P 0-90", "9P 0-90" and "13P 0-90" at 3 m/s, 4 m/s and 5 m/s. The parameters used for those simulations are exactly the same as the one used for the case of the previous section. Those numerical results are compared

and discussed on the basis of the experimental results.

3.4.1. Impact on 5P 0-90

The results of the experimental and numerical load-displacement curves and load-time curves are plotted in Figure 18 while damage maps are presented in Figure 19.

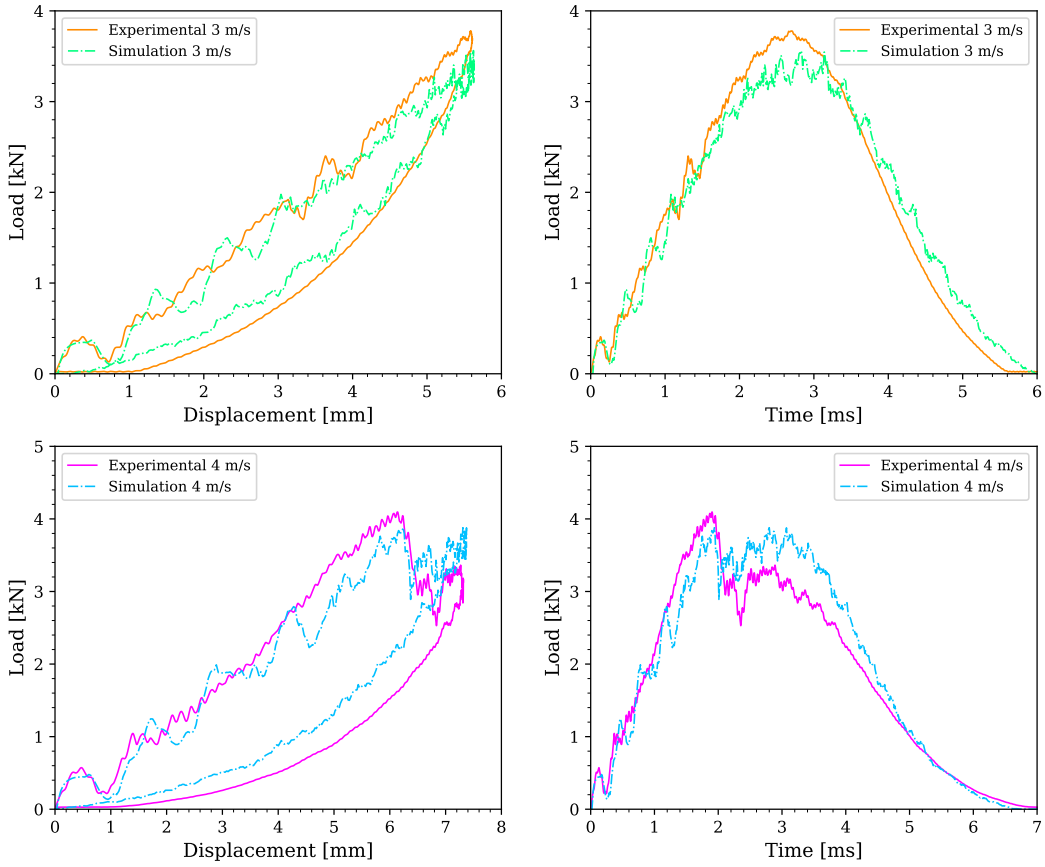

Figure 18: Load-displacement and load-time curves of the experimental tests and numerical simulations for 5P 0-90

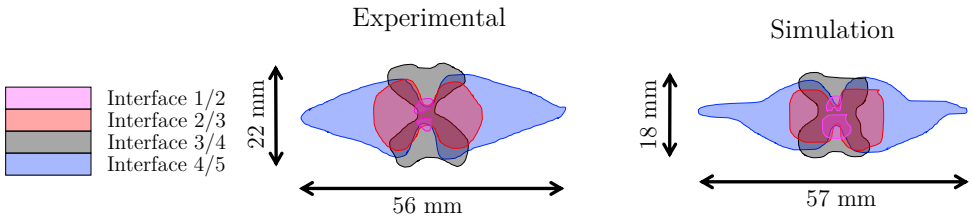

Figure 19: Cartography of the experimental and numerical delaminations for 5P 0-90 at 3m/s

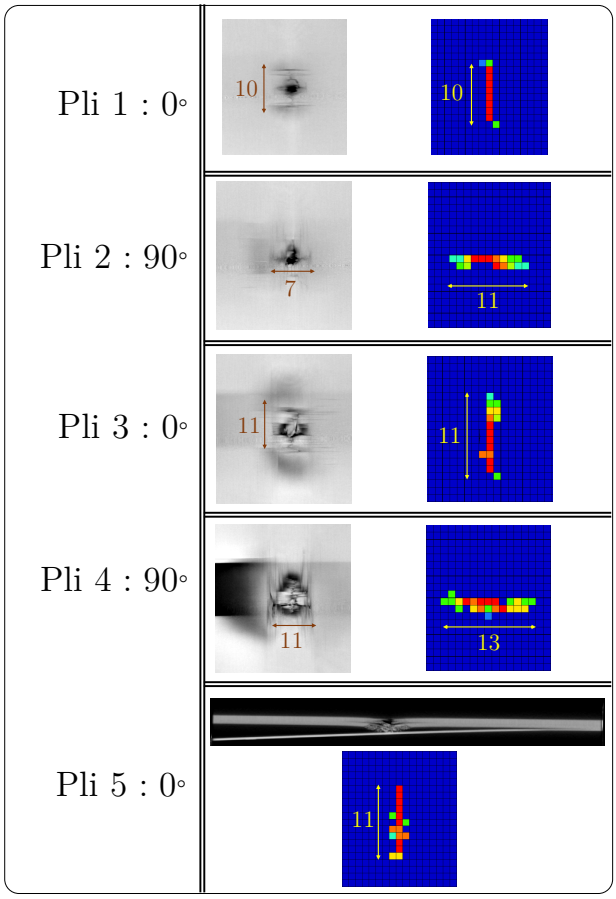

Figure 20: Experimental and numerical cartography of the fibres breakage for the 5P 0-90 at 4 m/s (in mm)

One notices that the numerical load-displacement curves correlate very precisely with the experimental ones. For 3 m/s, no significant event is visible in the curves and the delaminated areas are well represented by the model with an error on delaminated areas which is less than 15%.

However, the curve of 4 m/s shows a sudden drop at the end of the impactor motion which corresponds to fibres breakage through the thickness of the laminate (perforation). In Figure 21, only the rod elements are represented because at this velocity, it is more interesting to see fibres breakage than delaminated areas. This event is correctly captured by the model except for the broken rod elements in the 5^{th} ply. Indeed, experimentally, there is no broken fibres in this ply contrary to the simulation. Numerically, delamination is smaller than the experimental one as shown in Figure 21. The tomography shows that the delamination has propagated to one side of the plate whereas the simulation is not able to take into account the random behaviour that is linked to the heterogeneous defects inside the plate. Finally, in the simulation, for the reason that the plates borders are still stuck, the only way to dissipate the energy of the impactor is to break the rods.

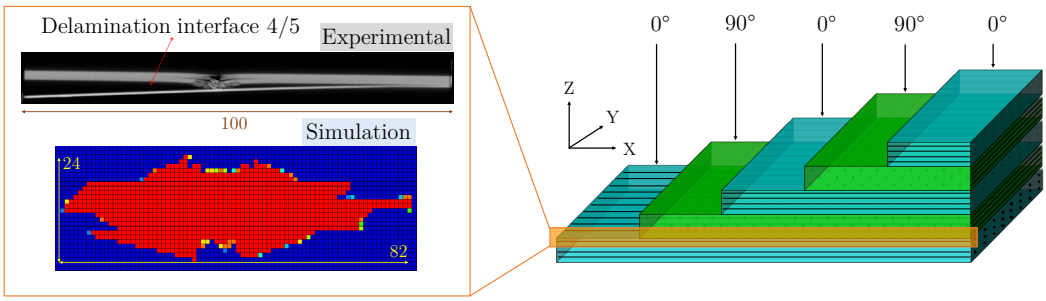

Figure 21: Delamination of the 4^{th} interface for the 5P 0-90 at 4 m/s

3.4.2. Impact on 9P 0-90

The results of the impacts on "9P 0-90" are shown in Figure 22 and Figure 23.

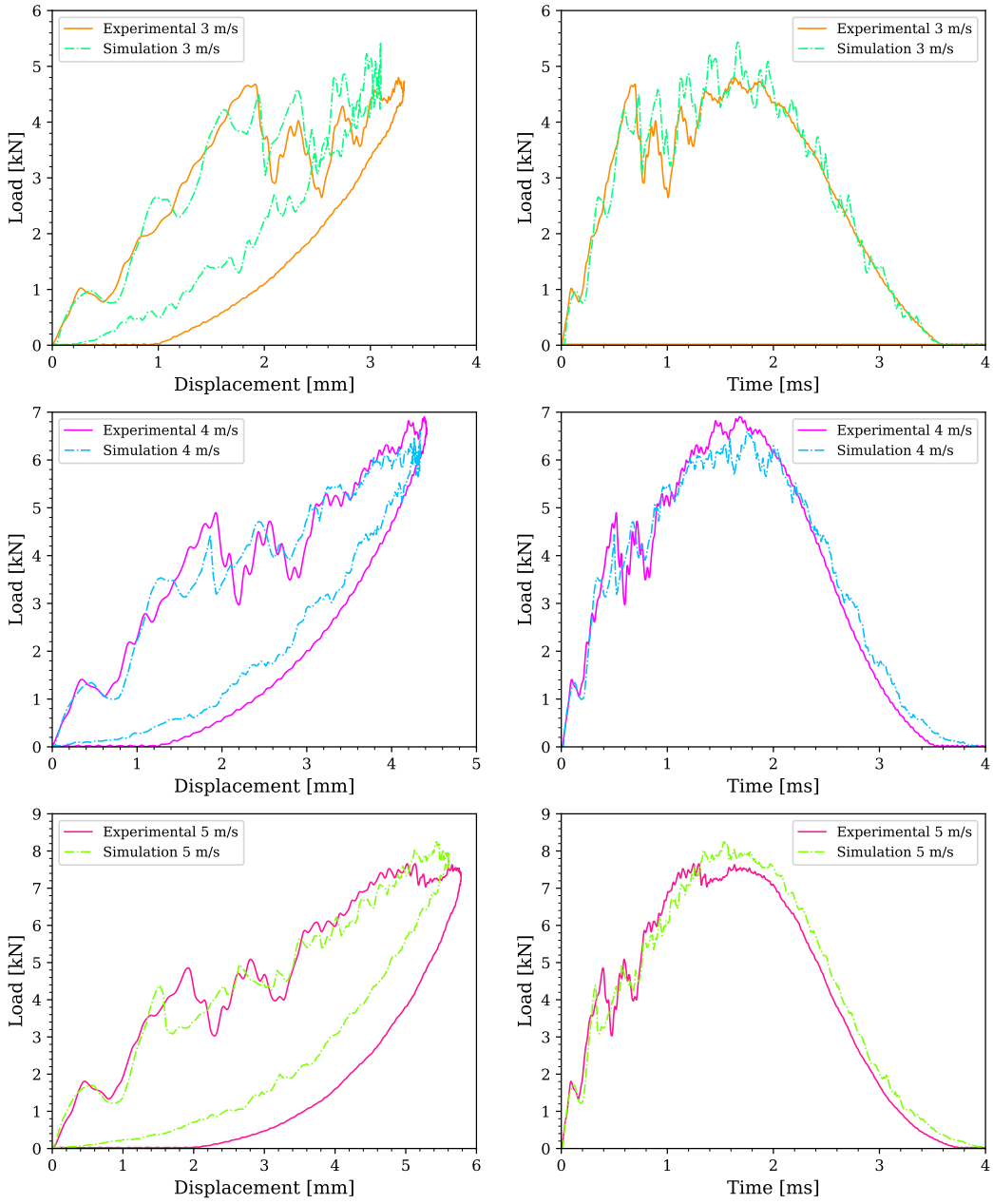

Figure 22: Load-displacement and load-time curves of experimental tests and numerical simulations for "9P 0-90" at 3 m/s, 4 m/s and 5 m/s.

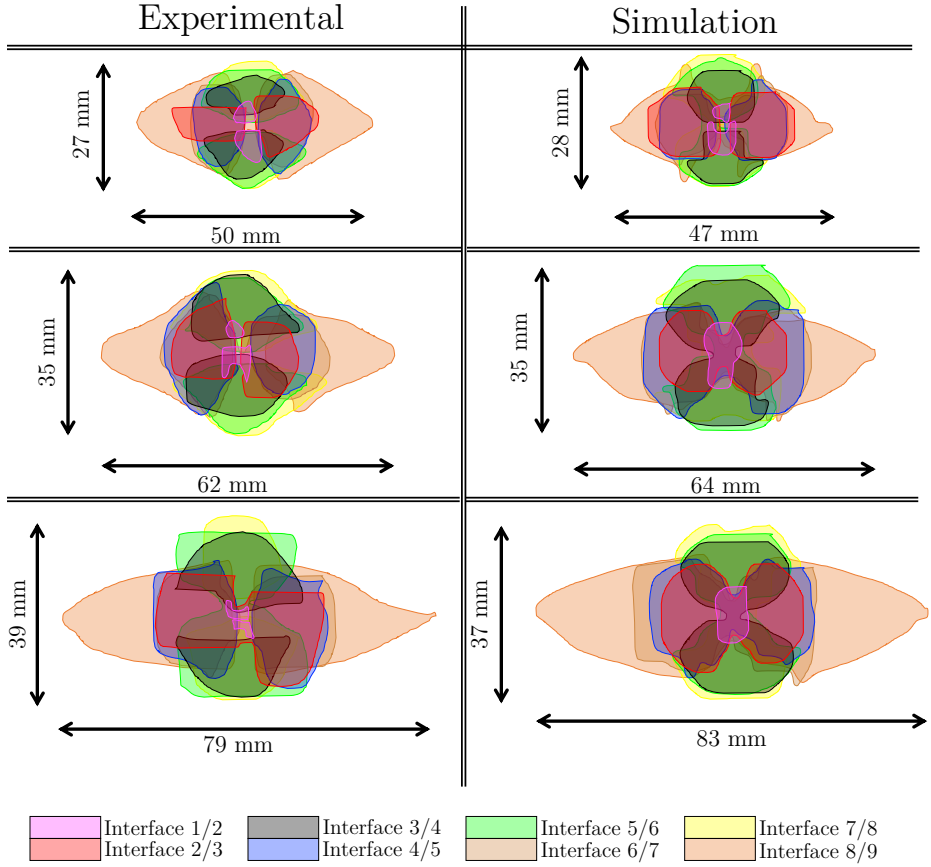

Figure 23: Cartography of experimental and numerical delaminations for "9P 0-90"

The results show that the model is very accurate in terms of dissipated energy and delamination representation. Indeed, the numerical sudden drop occurs at the same displacement as the experimental one and the post-drop stiffness is very similar between the experimental and numerical results. For all the cases, the relative error between the experimental and numerical tests is less than 7% in terms of delaminated areas and matrix crack lengths.

3.4.3. Impact on 13P 0-90

The comparison between the experimental and numerical results are gathered in Figure 24 and Figure 25 below.

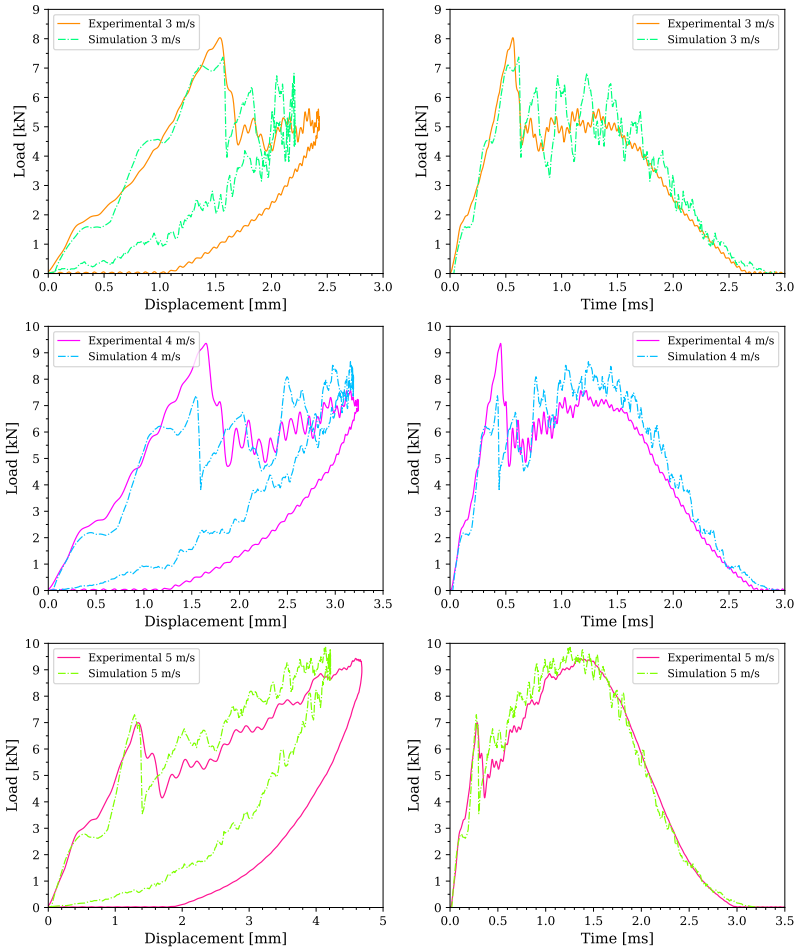

Figure 24: Load-displacement and load-time curves of experimental tests and numerical simulations for 13P 0-90

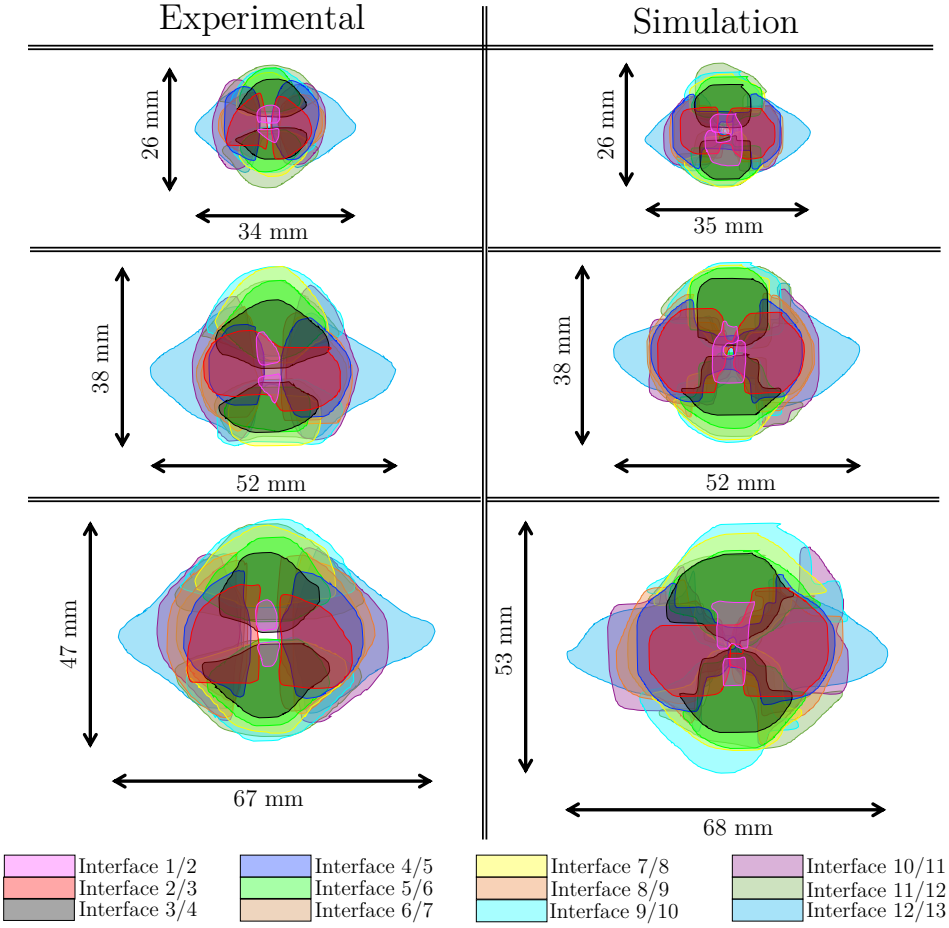

Figure 25: Cartography of the experimental and numerical delaminations for 13P 0-90

The numerical results presented below correlate also very well the experimental ones despite a slight variance on the load sudden drop at 4m/s.

3.4.4. Impact on 9P QI

The results of the impacts on "9P QI" are shown in Figure 26 and Figure 27.

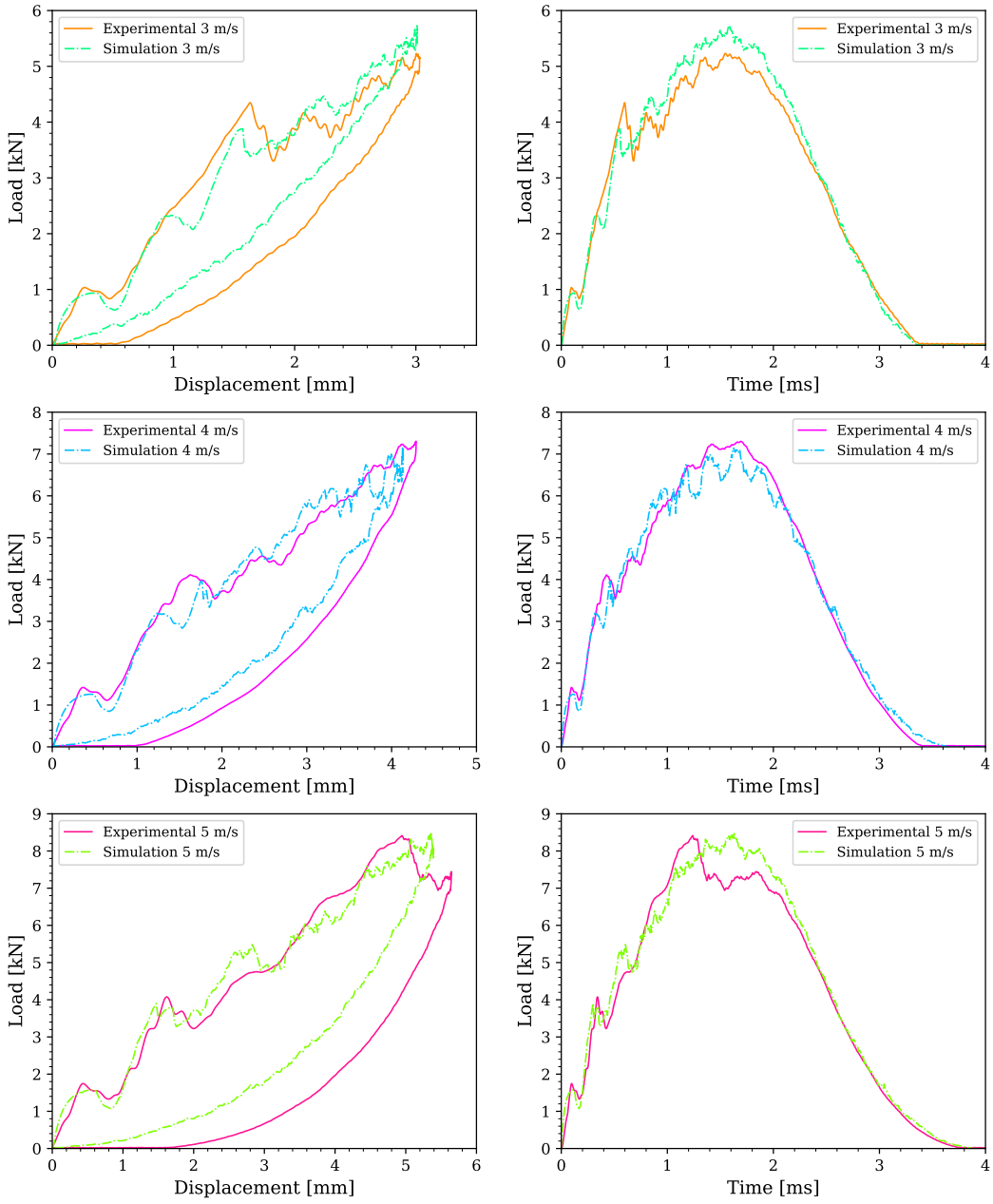

Figure 26: Load-displacement and load-time curves of experimental tests and numerical simulations for 9P QI

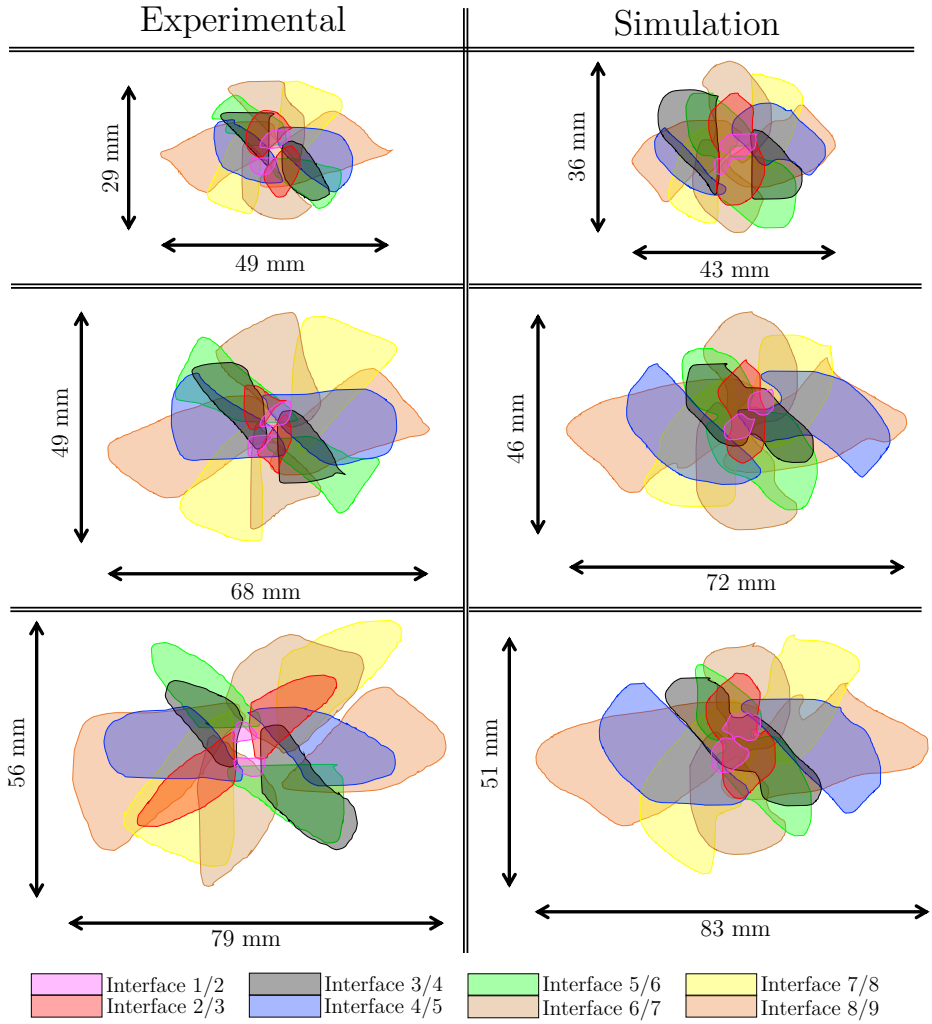

Figure 27: Cartography of the experimental and numerical delaminations for 9P QI

4. Discussion

The results presented previously show a very good correlation between experimental dissipated energies and the numerical ones. Moreover the mechanisms occur at the right time. Indeed, the sudden load drop is also caught

by the model thanks to the intralaminar interfaces. The impactor return is also well represented : this means that the remaining energy at this time, essential to the rise of the impactor, is also the same between the experimental and the numerical impacts. Moreover, the damages such as delamination are well predicted in terms of shapes and sizes.

These results can be compared to those that are given by other mature methods. Indeed, in terms of discrete damage representation, the *Discrete Ply Modeling Method* developed by [23] gives also very precise results. As this method allows an intralaminar damage / delamination coupling, it provides an accurate damage scenario. On the contrary,other models that do not represent precisely transverse cracks as described in [22] and [34], continuous models provide less detailed results.

5. Conclusion

This article presented the development of a new interface element in order to catch the behaviour due to transverse matrix cracking during low velocity impact on a composite structure. Accounting for these cracks, as it is commonly understood, is a key point in a predictive approach as they lead to the initiation of the delamination. The thicker the laminate, the more important this phenomenon. Comparisons between two models, namely with and without intralaminar interface, showed that the intralaminar element is essential to capture both the load-displacement curve and the cartography of damage mechanisms in thick laminates. Indeed, the sudden rupture of the interfaces is reproduced as the shapes and the sizes of the damages, only with the inter- and intra-laminar model.

This strategy requires the coupling of the intralaminar and the interlaminar damages. In fact, it allows to initiate a delamination exactly at the right time. This could not be done with the model without intralaminar interfaces, because the out-of-plane shear damaging mechanics was impossible. This, unfortunately, induces a complex meshing process in order to include the new element to the one already developed in the model. Despite this, this contribution to the semi-continuous strategy opens a new research field, on one side to better understand the initiation of the delamination and on the other side to improve prediction with thick laminates in real industrial structures. Moreover, it will be possible and interesting to use this model to estimate the post-impact resistance of composite structures and also to predict the state of damage of hybrid composites, constituted for example with unidirectional and woven plies.

Acknowledgement

This work was performed using HPC resources from CALMIP (Grant 2016-[P09105]).

References

[1] J. Aboissière, Propagation de dommages d'impact dans un matériau composite stratifié à fibres de carbone et résine époxyde, Ph.D. thesis, Université de Toulouse (2003).

[2] J.-H. Kim, Identification de cartes d'endommagement de plaques composites impactées par la méthode des champs virtuels., Ph.D. thesis, Ecole Nationale Supérieure des Arts et Métiers (2008).

[3] O. Sensing, D. VI (Eds.), Barely visible impact damage detection and location on composite materials by surface-mounted and embedded aerospace-compatible optical fibre Bragg grating sensors, no. 113540E, SPIE Photonics Europe, Optical Sensing and Detection VI, 2020.

[4] A. Wronkowicz-Katunin, A. Katunin, K. Dragan, Reconstruction of barely visible impact damage in composite structures based on non-destructive evaluation results, Sensors.

[5] R. . Wisheart, Review of low-velocity impact properties of composite materials, Composite Part Applied Science Manufacture 27 (12) (1996) 1123–1131.

[6] W. Cantwell, J. Morton, Comparison of the low and high velocity impact response of cfrp, Composites 20 (6) (1989) 545–551.

[7] R. Olsson, Mass criterion for wave controlled impact response of composite plates, Composites Part A : Applied Science and Manufacturing.

[8] J. Morton, W. Cantwell, The impact resistance of composite materials : a review, Composites 22 (5) (1991) 347–362.

[9] Liu, Impact-induced delamination : a view of bending stiffness mismatching, Journal of Composite Materials 22 (7) (1998) 674–692.

[10] S. Abrate, Impact on laminated composites : recent advances, Applied Machanical Review 47 (11) (1994) 517–544.

[11] J. Abrate, Impact on composite structures, Cambridge University.

[12] H. Choi, F. Chang, A model for predicting damage in graphite/epoxy laminated composites resulting from low-velocity point impact, Journal of Composite Materials 26 (1992) 2134–2169.

[13] P. Hu, An experimental study on the influence of intralaminar damage on interlaminar delamination properties of laminated composites, Composites Part A : Applied Science and Manufacturing 131 (105783).

[14] G. Minak, M. Fotouhi, M. Ahmadi, Dynamic Deformation, Damage and Fracture in Composite Materials and Structures, ScienceDirect, 2016.

[15] E. González, P. Maimí, P. Camanho, C. Lopez, N. Blanco, Effects of ply clustering in laminated composite plates under low-velocity impact loading, Composite Science and Technology 71 (2011) 805–817.

[16] S. Abrate, Cohesive zone models and impact damage predictions for composite structures, Meccanica 50 (10) (2015) 2587–2620.

[17] Wisnom, Modeling discrete failures in composites with interface elements, Composite Part A : Applied Science and Manufacturing 41 (7) (2010) 795–805.

[18] A. Caporale, R. Luciano, E. Sacco, Micromechanical analysis of interfacial debonding in unidirectionnal fiber reinforced composites, Computers and Structures 84 (2006) 2200–2211.

[19] A. Orifici, I. Alberdi, R. Thomson, J. Bayandor, Compression and post-buckling damage growth and collapse analysis of flat composite stiffened panels.

[20] S. Tsai, E. Wu, A general theory for anisotropic materials, Journal of Composite Materials 80 (1971) 58–80.

[21] S. Hashemi, A. Kinloch, J. Williams, The analysis of interlaminar fracture in uniaxial fiber-polymer composites, Proceedings of the Royal Society of London (1990) 173–199.

[22] P. Ladevèze, G. Lubineau, On a damage mesomodel for laminates : micromechanics basis and improvement, Mechanics of Materials 35 (8) (2003) 763–775.

[23] C. Bouvet, B. Castanié, M. Bizeul, J. Barrau, Low velocity impact modelling in laminate composite panels with discrete interface elements, International Journal of Solids and Structures 46 (14-15) (2009) 2809–2821.

[24] F. Aymerich, F. Dore, P. Priolo, Prediction of impact-induced delamination in cross-ply composite laminates using cohesive interface elements, Composites Science and Technology 68 (12) (2007) 2383–2390.

[25] D. Feng, F. Aymerich, Finite element modelling of damage induced by low-velocity impact on composite laminates, Composite Structures 2014 (2013) 161–171.

[26] Y. Shi, C. Pinna, C. Soutis, Modelling impact damage in composite laminates: A simulation of intra- and inter-laminar cracking, Composites Structures 114 (2014) 10–19.

[27] A. Airoldi, C. Mirani, L. Principito, A bi-phasic modelling approach for interlaminar and intralaminar damage in the matrix of composite laminates, Composite Structures 234.

[28] R. Ren, J. Zhong, G. Le, D. Ma, Research on intralaminar load reversal damage modeling for predicting composite laminates' low velocity impact responses, Composite Structures 220 (2019) 481–493.

[29] H. Kahla, Z. Ayadi, F. Edgren, A. Pupurs, J. Varna, Statistical model for initiation governed intralaminar cracking in composite laminates during tensile quasi-static and cyclic tests, International Journal of Fatigue 116 (2018) 1–12.

[30] P. Navarro, Etude de l'impact oblique à haute vitesse sur des structures en sandwich composite : application aux pales d'hélicoptère, Ph.D. thesis, Université Toulouse 3 Paul Sabatier (2010).

[31] F. Pascal, P. Navarro, S. Marguet, J. Ferrero, On the modelling of low to medium velocity impact into woven composite materials with a 2d semi-continuous approach, Composite Structures 134 (2015) 302–310. doi:10.1016/j.compstruct.2015.08.067.

[32] B. Mahmoud, M. Colungo, P. Navarro, S. Marguet, I. Tawk, J. Ferrero, Semi-continuous strategy for the modeling of damage mechanisms in unidirectional composites under low velocity impacts, Composite Structures Part B. doi:10.1016/j.compositesb.2017.07.014.

[33] J. Aubry, Etude expérimentale et numérique d'impact sur structures : application aux pales d'hélicoptères, Ph.D. thesis, Université Fédérale de Toulouse (2013).

[34] E. Abisset, Un mésomodèle d'endommagement des composites stratifiés pour le virtual testing : identification et validation., Ph.D. thesis, École Normale Supérieure de Cachan (2012).